The Yucatan Minipig as a Potential Preclinical Animal Model for Carpal Bone Arthroplasty

Quianna M. Vaughan[1], Sophia Sordilla[1], Amy Morton[1], Douglas C. Moore[1], Edward Akelman[1], Joseph J. Crisco[1]
[1]Department of Orthopaedics, Warren Alpert Medical School of Brown University and Rhode Island Hospital, Providence, RI
Email: quianna_vaughan@brown.edu

Disclosures: Q.M. Vaughan: None. **S. Sordilla**: None. **A.M. Morton**: None. **D.C. Moore:** None, **E. Akelman**: None **J.J. Crisco**: None.

INTRODUCTION: Hand and upper extremity injuries are a large contribution to common orthopedic injuries and often lead to painful osteoarthritis and disability which minimizes quality of life. Patients who suffer from wrist injuries, namely fractures, carpal instability, and ligament injury, commonly develop severe osteoarthritis (OA). The successful treatments and outcomes for injuries to the hip, knee, and shoulder are attributed to the evaluation of extensive *in vitro* and *in vivo* studies, as compared to the wrist. As a result, the development of innovative therapeutics for carpal OA has been hindered due to a lack of data and an insufficient understanding of the anatomical and biomechanical complexity of the wrist. Our overall goal is to establish the Yucatan minipig as a preclinical animal model to aid in the development and validation of innovative therapeutics and hemiarthroplasties to treat carpal bone pathologies associated with ligament injuries and severe OA. The Yucatan minipig carpus is a potential preclinical animal model for the human carpus because of the similarities in size, anatomy, bone, and cartilage physiology (Fig. 1). In a previous study, the radial carpal bone (RCB) was used as a model for scaphoid nonunion due to the location of the bone and analogous nutrient vessels into the dorsal and volar poles of the RCB that are similar to the scaphoid in humans [1]. Our specific aim is to quantitatively analyze the morphology of the RCB to determine the feasibility of employing specimen weight as a predictive measure for RCB size to assist in the selection of a carpal bone arthroplasty with optimal dimensions for successful implantation in *in vivo* studies.

METHODS: A total of 22 Yucatan forelimbs (18-20 months in age), 8 females and 3 males ranging between 49-61 kg in weight, were imaged with a clinical CT scanner to establish our porcine database. A total of 11 RCBs were resected from this specimen group and scanned using a MicroCT40 desktop microcomputed tomography (µCT) system (Scanco Medical. Brüttisellen, CH). The system was set to 70KVp and 114 µA, and an isometric voxel size of 30 um. The clinical CT-scanned RCBs were segmented using Mimicsv22 (Materialise, Leuven, Belgium) and exported as triangular surface models. The subchondral bone and articular cartilage were segmented from µCT-scanned RCBs. The inertial coordinate system (ICS) was calculated for each clinical CT model using custom MATLAB scripts (Mathworks, US) assuming uniform density and using geometric mean to define the ICS centroid. Anatomical specificity and sign of the computed ICS vectors were standardized to orient dorsal, proximal, and ulnar (facing the intermediate carpal bone). Bone models were imported to Geomagic Wrap (Geomagic Wrap; 3D Systems, SC) to smooth the surface of the RCB and compute bone volume, surface area, and bounding box dimensions. Articular cartilage thickness was defined as the distance between the articular cartilage and subchondral bone meshes (Fig 2). Mean articular cartilage thickness and standard deviation were calculated for each bone. Mean articular cartilage thickness was averaged across the 11 collected RCBs. Linear regression was used to determine correlations between specimen weight and bone volume, and specimen weight and bounding box dimensions.

RESULTS: The average RCB volume was 1570.7±182.4 mm^3 with an average surface area of 789.9±60.9 mm^2. The bounding box dimensions had an average length of 19.6±0.9 mm in the volar-dorsal direction (x), 16.1±0.7 mm in the proximal-distal direction (y), and 11.4±0.8 mm in the radial-ulnar direction (z). A significant correlation existed between specimen weight and bone volume, specimen weight and bone length in the volar dorsal direction, and specimen weight and bone length in the radial-ulnar direction ($p<0.0001$, $R^2 = 0.724, 0.593, 0.560$, respectively). In the proximal-distal direction, the relationship between specimen weight and bone length exhibited an R^2 value of 0.265 and a p-value of 0.0169. The mean articular cartilage thickness across RCBs for the distal facet was 0.3±0.03 mm, while the proximal facet displayed a mean articular cartilage thickness of 0.3±0.04 mm. The articular cartilage thickness across all RCBs spanned a range from 0.24 to 0.38 mm.

DISCUSSION: Our specific aim was to analyze the morphology of the RCB to determine if specimen weight can be used as a predictive measure for RCB size. We found a modest correlation between specimen weight and bone volume, and specimen weight and bounding box dimensions. However, the correlations support specimen weight as an indicator of the approximate range of viable implant sizes. Comparing averaged bone volumes of the minipig RCB (1570.7±182.4 mm^3) to averaged volume of the human scaphoid (2390.1±673.6 mm^3) [2], the human scaphoid is consistently larger. A limitation of this study includes the effect CT resolution may have on bone volume and bounding box dimensions. Another limitation of this study is all specimens were skeletally immature, and once the Yucatan minipig is matured, the specimen weight may continue to increase while the bone volume remains consistent. A final limitation of this study is the small sample size of our Yucatan minipig database.

SIGNIFICANCE: The establishment of a preclinical animal model for the human wrist will advance therapeutics aimed at restoring normal carpal biomechanics and mitigating the progression of osteoarthritis, which will contribute to the data-driven development of human carpal bone arthroplasty.

ACKNOWLEDGEMENT: Supported in part by NIH/NIAMS under award number R21AR082130.

REFERENCES: [1] Behrends, *J Funct Biomater*, 2015. [2] Crisco, *J Hand Surg*, 2005.

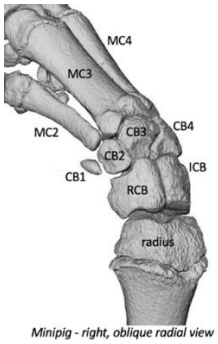

Human	Minipig
metacarpals (MC1-5)	metacarpals (MC1-4)
Trapezium (Tpm)	1st carpal bone (CB1)
Trapezoid (Tpd)	2nd carpal bone (CB2)
Capitate (Cap)	3rd carpal bone (CB3)
Hamate (Ham)	4th carpal bone (CB4)
Scaphoid (Sca)	Radial carpal bone (RCB)
Lunate (Lun)	Intermediate carpal bone (ICB)
Triquetrum (Trq)	Ulnar carpal bone (UCB)
Pisiform (*not visible*)	Accessory carpal bone (*not visible*)

Figure 1. Bone model segmentation of the Yucatan minipig forelimb CT. Table of Yucatan minipig and human bone analogs.

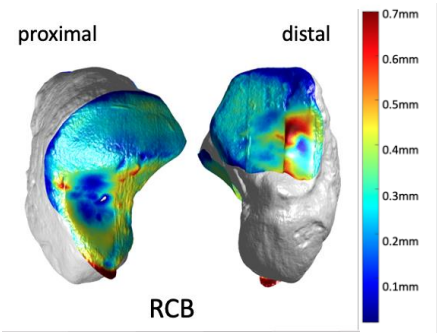

Figure 2. Thickness of articular cartilage indicated by a colormap for the radial articulating facet (left) and distal carpal row articulating facet (right) of an RCB.

Approach to Evaluate Femoral Cartilage Thickness Based on Patient Geometry

Crystal J. Murray,[1,2] Janine Molino,[1,2,3] Meggin Costa,[1,2], Braden C. Fleming,[1,2] Jillian E. Beveridge[1,2]
[1]Rhode Island Hospital, Providence, RI, [2]Brown University, Providence, RI, [3]Brown University, Biostatistics Providence, RI
crystal_murray@brown.edu

Disclosures: Braden C. Fleming (Miach Orthopaedics, American Journal of Sports Medicine); Other authors (N)

INTRODUCTION: Loss of tibiofemoral cartilage is a hallmark feature of posttraumatic osteoarthritis progression (PTOA) following anterior cruciate ligament (ACL) injury and subsequent ACL reconstruction surgery (ACLR);[1,3] however, biological sex-based differences in cartilage thickness are known to exist.[2] As these baseline characteristics could contribute to the varied sequelae observed following ACLR, we sought to test whether cartilage thinning was sex-dependent in a subset of patients participating in a longitudinal clinical trial evaluating outcomes after ACLR (NCT00434837). To do so, we developed an approach to quantify sub-regional medial femoral condyle (MFC) cartilage thickness that could be scaled to account for differences in knee size. We hypothesized that: 1) MFC cartilage in uninjured female controls would be thinner than in uninjured male controls; and 2) MFC cartilage thickness in ACLR patients (10-15 years post-surgery) would be thinner than uninjured controls.

METHODS: Nine ACLR patients (4M/5F; 10-15 years post-surgery; mean age 34±10.5 years) and 12 uninjured controls (7M/5F; no history of knee injury; mean age 38±7.4 years) participated in this IRB-approved study. Tibiofemoral cartilage was segmented from magnetic resonance (MR) images acquired using a 3D fast low angle shot (FLASH) sequence (RT/ET/FA: 20ms/7.6ms/12°; slice thickness/gap: 1.5/0mm; 0.313x0.313x1.5mm voxel size). Femoral bony geometry was segmented from images acquired from computerized tomography (CT) scans (80kV, smart mA, 0.293x0.293x0.625mm voxel size). The cartilage and bone segmentations were used to generate 3D mesh models that were smoothed and remeshed using commercial software (Mimics; Materialise, Geomagic Wrap; 3D Systems). A local coordinate system was generated from the femoral geometry using an established approach.[4] The cartilage models were aligned in the femoral coordinate system using an iterative closest point algorithm (RMS error: 1.53±0.33mm). Cartilage thickness was mapped from the subchondral bone surface to the articular surface using a k-nearest neighbor search algorithm (MATLAB R2022b; Mathworks). The location of the femoral notch was used to delineate medial and lateral condyles. Based on the width and curvature of the condylar cartilage, 24 proportionally distributed MFC sub-regions were generated (mean sub-region size across patients: 2.72±0.46mm^2; Fig 2). Mixed models were used to test the study hypotheses. Pairwise comparisons were conducted via orthogonal contrasts. The Holm test was used to maintain a two-tailed familywise alpha at 0.05.

RESULTS: Cartilage thickness was not different (p=0.069) between female and male healthy controls (2.13mm, 95% CI=1.83-2.43 versus 2.54mm, 95% CI=2.22-2.87); however in a pooled analysis of both ACLR and Controls, females had significantly (p=0.004) thinner MFC cartilage (2.26mm, 95% confidence interval (CI)=1.99-2.54 versus 2.76mm, 95% CI = 2.57-2.95) with a trend towards a group X sex interaction [F(1, 483)=0.23, p=0.063] (Fig 1). A significant interaction effect between sex and location was detected in both the Control-only [F(10, 230)=2.83, p=0.003] and pooled analyses [F(19, 437)=22.05, p<.0001]. In the pooled analysis, females had thinner cartilage across 13/24 sub-regions which were primarily coincident with the weight-bearing region of the condyle (sub-regions #7-18). ACLR patients tended (p=0.056) to have thicker MFC cartilage (2.68mm, 95% CI=2.42-2.95 versus 2.34mm, 95% CI=2.10-2.57), with a significant interaction effect between group and sub-region [F(19, 437)=22.05, p<.0001; Fig 3). Although limited by statistical power, 7/24 sub-regions were significantly different between ACLR and Controls before adjusting for multiple comparisons; these regional trends in thickened cartilage coincided with the anterolateral region of the femoral notch (sub-regions #3 & 6) and central weight-bearing regions (sub-regions #14, 17, 19 20, 24).

DISCUSSION: Trends in our results were consistent with the literature describing females having thinner tibiofemoral cartilage than males,[2] but did not warrant separate analyses for male and females as we originally hypothesized. Also contrary to our hypothesis, our results highlighted a trend towards ACLR patients having thicker cartilage than healthy controls. These results suggest that even 10+ years after ACLR surgery, these patients present with cartilage swelling rather than thinning at this stage. Cartilage thickness significantly differed by sub-region in all analyses. While raw p-values suggested that some sub-regions were preferentially affected in ACLR patients, we were limited by statistical power. Nevertheless, the sub-regional approach used to quantify cartilage thickness differences revealed potentially clinically relevant cartilage thickening that likely would have been overshadowed if expressed as a mean of the entire surface. Further, the detected regional trends in cartilage thickening align with those previously reported,[5] giving some confidence in the trends.

SIGNIFICANCE/CLINICAL RELEVANCE: Coupled with AI-based algorithms for automatic cartilage model generation, the approach could be applied to larger cohorts to monitor cartilage changes earlier in the disease trajectory when interventions may be more effective.

REFERENCES: [1] Ichiba, A., et al. Arch Orthop Trauma Surg 129 (2009); [2] Otterness, I. G., et al. Osteoarthritis Cartilage (2007); [3] Erhart-Hledik, J., et al. J Orthop Res. (2019); [4] Miranda, D., et al. J Biomech. (2010) [5] Coleman, J. L., et al. J Biomech (2013)

ACKNOWLEDGEMENTS: NIH NIAMS K99/R00-AR069004; R01-AR047910; R01-AR074973; NIGMS P30-GM122732; Lucy Lippitt Endowment

IMAGES AND TABLES:

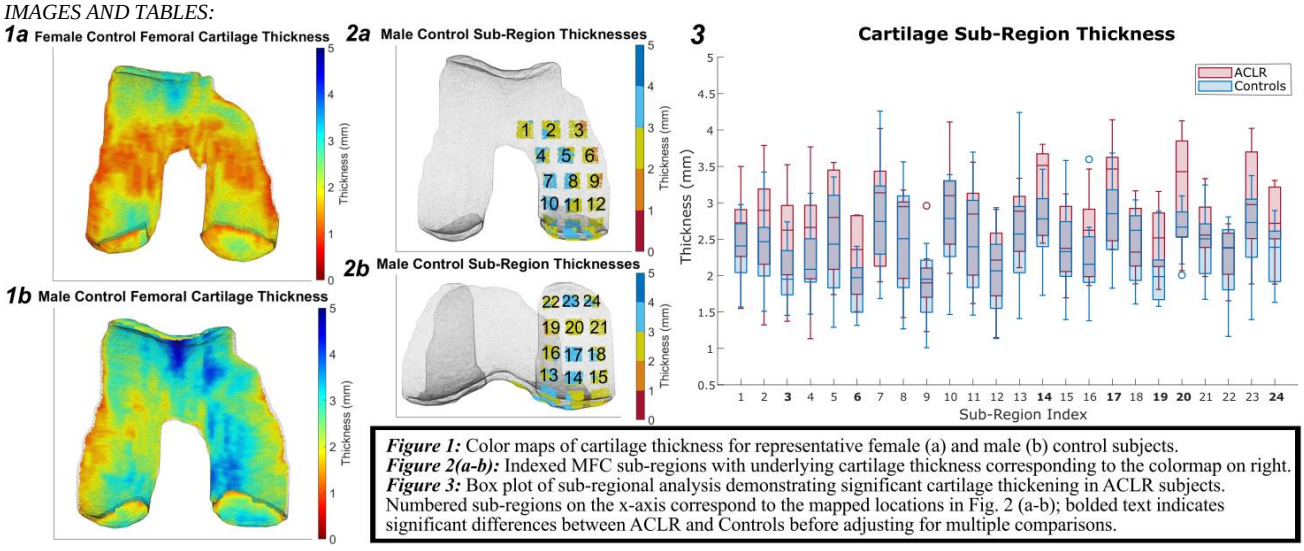

Figure 1: Color maps of cartilage thickness for representative female (a) and male (b) control subjects.
Figure 2(a-b): Indexed MFC sub-regions with underlying cartilage thickness corresponding to the colormap on right.
Figure 3: Box plot of sub-regional analysis demonstrating significant cartilage thickening in ACLR subjects. Numbered sub-regions on the x-axis correspond to the mapped locations in Fig. 2 (a-b); bolded text indicates significant differences between ACLR and Controls before adjusting for multiple comparisons.

***In Vitro* Biomechanics of the Healthy Thumb CMC Joint**

Josephine M. Kalshoven[1], Rohit Badida[1], Douglas C. Moore[1], Joseph J. Crisco[1]
[1]Department of Orthopaedics, Warren Alpert Medical School of Brown University and Rhode Island Hospital, Providence, RI
Email: Josephine_Kalshoven@brown.edu

Disclosures: J.M. Kalshoven: None. **R. Badida**: None. **D.C. Moore**: None. **J.J. Crisco**: None.

INTRODUCTION: Studies have found that active and passive ranges of motion (ROM) are reduced in thumb carpometacarpal (CMC) joint osteoarthritis (OA), yet the underlying causes for this reduction remain unclear [1]. Osteophyte growth and ligament property changes associated with progressive OA have been hypothesized to affect CMC ROM, yet no study has confirmed a causal relationship. An *in vitro* biomechanical assessment would allow for prescribed, directional load application, shedding light on inherent stabilizing structures. The aim of this work was to determine the *in vitro* ROM and stiffness in 26 distinct directions of thumb CMC motion for specimens without OA using a musculoskeletal simulator.

METHODS: Ten fresh-frozen human forearms (5M, 5F, 27-62 yrs.) with less than 150 mm^3 of rimming trapezial osteophytes were sectioned proximally at the midshaft of the radius/ulna. All bones distal to the carpus were removed, except for the first metacarpal (MC1) and the proximal head of the second metacarpal (MC2). An optical motion sensor consisting of 6 infrared markers (NDI) was rigidly mounted via two k-wires to the radial surface of the trapezium (TPM) to provide a reference frame for data reporting. CT scans of all specimens were acquired and post-processed to generate TPM- and MC1-based anatomical coordinate systems, as described previously [2]. Briefly, MC1 and TPM bone coordinate systems (CS) were computed based on directions of principal curvature of the articular surfaces [3] and, for the MC1, its proximal-distal inertial axis. CS axes were directed volarly (+x), proximally (+y), and radially (+z). Each specimen was mounted to a six-axis industrial robot (KUKA KR 6 R700) with the radius and ulna affixed to the robot base and the MC1 to the robot end effector. Specimen-specific CT-generated coordinate systems were registered in the robot space and joint coordinate systems were constructed using simVITRO (Cleveland Clinic) [2]. The flexion-extension axis (Z axis) was fixed in the TPM, the pronation-supination axis (Y axis) was fixed in the MC1, and a floating abduction-adduction rotation axis (X axis) was defined perpendicular to the two body-fixed axes (**Fig. 1**). All ROM tests began from CMC joint neutral, defined at 1) 0º MC1 rotation in flexion, extension, abduction, adduction; 2) 2 N proximal compression for joint contact, and 0 N volar, dorsal, radial, ulnar joint forces; 3) 0 Nm torque in pronation and supination. Tests were performed in 26 distinct directions of MC1 rotation: pronation, supination, and 24 directions comprising a ROM envelope (the orthogonal anatomically-defined directions of flexion, extension, abduction, and adduction, as well as 20 coupled directions at 15-degree increments from the orthogonal directions). In each of the 26 rotational directions, maximum ROM was determined by rotating the MC1 at 1 º/s until a resultant RMS torque of 1 Nm was achieved. Joint forces were fixed at 0 N volarly, dorsally, radially, and ulnarly, and in 2N of joint compression, with translations allowed as necessary to main the fixed force state. TPM motion was recorded throughout the duration of each test via the rigidly-attached TPM sensor. Torque-rotation curves were analyzed from 6 DOF kinematics and kinetics of the MC1 with respect to the TPM to determine rotational ROM at 1 Nm. The portion of the torque/rotation curve with a torque greater than 0.5 Nm was fit with a linear regression model. The slope of this model was recorded as the final stiffness K (Nm/º). The principal directions of motion were computed as eigenvectors of the envelope of ROM and stiffness.

RESULTS: The major principal axis of the mean rotational ROM envelope for the CMC joint was oriented oblique to the primary axes of flexion-extension and abduction-adduction, angled at 29.2º from pure adduction toward extension (**Fig. 2A**). The ROM in this principal axis direction was 49.3 ±13.6º, which was significantly greater than the ROM recorded in the primary directions of extension (28.4±5.2º, $p<0.05$) and abduction (29.0±10.6º, $p<0.01$). The major principal axis of the mean rotational stiffness envelope was oriented approximately orthogonal to the mean ROM envelope at 54.1º from pure flexion in the direction of adduction (**Fig. 2B**). Stiffness was greatest at 45º from flexion toward abduction (0.14±0.03Nm/º) and least at 30º from extension toward adduction (0.07±0.03 Nm/º). Pronation ROM was 49.0 ± 18.8º, supination ROM was 34.2±8.1º, and the combined pronosupination ROM was 82.6± 17.2º. Pronation stiffness was 0.07±0.03 Nm/º and supination stiffness was 0.09± 0.02 Nm/º.

DISCUSSION: We observed that the major principal direction of the thumb CMC range of motion was oriented along the adduction-extension to abduction-flexion axis, which is the path through which the thumb carries out the functional motions of opposition and retroposition. Accordingly, the major principal axis of thumb CMC joint stiffness was oriented approximately orthogonal to the ROM principal axis. Pronation and supination stiffness values were consistent with those reported by Shrivastava et al [4]. This study is novel in its presentation of the thumb range of motion envelope *in vitro*. Traditionally, thumb ROM is characterized by the primary anatomical directions of flexion, extension, abduction, and adduction. However, our data indicate that the greatest ranges of motion of the thumb lie oblique to these primary axes. This pattern is consistent with healthy *in vivo* thumb circumduction data [1]; however, our ROM values are larger than those reported *in vivo* [5]. This is likely due to specimen preparation (i.e., missing MC2, musculature) and an externally applied torque that may be greater than the torque at the position a subject would usually consider their maximal range of motion.

SIGNIFICANCE: These results provide healthy CMC biomechanical data that can be used as a benchmark for understanding the mechanics of the pathological and post-operative joint. Additionally, these results support the feasibility of testing CMC biomechanics across a spectrum of osteoarthritis presentation, which would build a more complete understanding of the interplay of pathology and joint mechanics.

REFERENCES: [1] Gehrmann, *J Hand Surg Am*, 2010. [2] Badida, *J Biomech Eng*, 2020. [3] Halilaj, *J Biomech*, 2013. [4] Shrivastava, *J Hand Surg*, 2003. [5] Crisco, *J Hand Surg Am*, 2015.

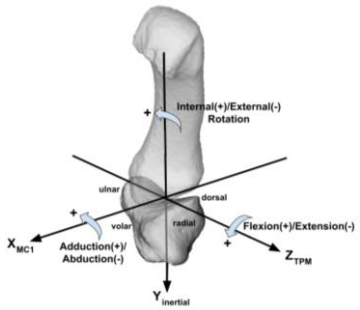

Figure 1. CMC coordinate axes and rotations.

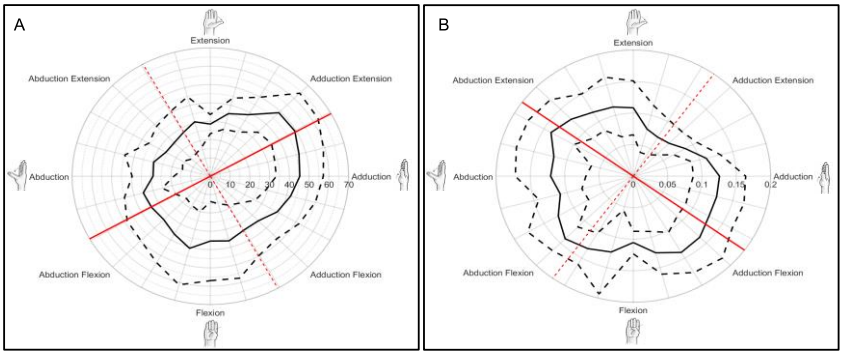

Figure 2. ROM and Stiffness Envelopes. (**A**) Mean (±1SD) Range of Motion (°) at 1 Nm in 24 directions. (**B**) Mean (±1SD) Final Stiffness (°/Nm) in 24 directions. Major principal axes of the mean envelopes in solid red, minor principal axes in dotted red.

Inductive Powering Profile of an Instrumented Trapezium for Measuring *In Vivo* Loads at the Base of the Thumb

Amy M. Morton[1], Melanie M. Baker[1], Petar V. Horvatic[2], Courtney P. Medeiros[2], David A. Durfee[2],
Daniel G. McDermott[1], Douglas C. Moore[1], Joseph J. Crisco[1]
[1]Department of Orthopaedics, Rhode Island Hospital and Warren Alpert Medical School of Brown University, Providence, RI
[2]Bay Computing, Cranston, RI
Email: joseph_crisco@brown.edu

Disclosures: Morton: None. Baker: None. Horvatic: None. Medeiros, None. Durfee: None. McDermott: None. Moore: None. Crisco: None.

INTRODUCTION: We are developing an instrumented replacement trapezium implant (iTrapz, Fig. 1) capable of measuring loads at the base of the thumb *in vivo*. The implant will be used in patients whose trapeziums have been resected as part of their treatment for advanced trapeziometacarpal arthritis. Our long-term goal is to directly record the loads at the base of the thumb during normal hand function, with the goal of informing clinical treatment, advancing arthroplasty design, and refining the inputs for musculoskeletal modeling. The iTrapz will be powered inductively, via a transmitting coil embedded in a tight-fitting glove with mating receiving electronics installed in the trapezium-shaped housing. Inductive power transmission is most efficient when the transmitting and receiving coils are co-axial, parallel, and in close proximity. In this study, we sought to determine the envelope of coil separation and alignment that would yield adequate inductive power transmission.

METHODS: The external housing of the iTrapz was designed using a statistical shape model generated from healthy CT segmented trapezia (N=46), scaled to the 95th percentile bone volume (male volunteer, approx. 17x15x25mm^3). Made of laser sintered Ti6Al4V, the housing included a circular, dorsally directed boss to fixture the ferrite-encased receiving coil. The location of the receiving coil was approximated by its exterior circular receiving "window" (Fig. 2 green disk). Our prototype inductive power transmission system included a pair of stacked 4-layer, 20 mm X 2.7 mm wireless charging coils (TDK WT202080-28F2-G) and a pair of concentric receiving coils (Wurth 760308101217 and 760308101221) in an uncoated PC200 ferrite core (TDK B65803J0000R608). The transmitting coil was powered at 3V with up to 3A of current. Induced current in the receiving coil was rectified with a matching capacitor bridge rectifier consisting of 4 low-forward-voltage-drop Schottky didoes, and a 3.3V Zener protection diode. Output voltage was measured with a Fluke 189 True RMS Multimeter. Transmitting coil and receiving window positions were quantified using a four-camera Qualisys optical motion capture (OMC) system (Oqus 500, 200Hz) and two custom 3D marker appliances: 1) a wand designed to facilitate moving of the transmitting coil and 2) a rigid mount for the iTrapz prototype (negative impression of the iTrapz volar surface, window facing up) (Fig. 2). The transmitting coil wand was manually elevated, rotated, and translated while marker positions were captured and synchronized with the receiving voltage. OMC and voltage data were acquired at 200Hz (Measurement Computing, integrated into Qualisys). The position of the transmitting coil relative to the receiving coil window was quantified by calculating a) Separation: the vertical distance from the transmitting coil center to the window center, and b) Alignment: the distance from window center to the projection of the coil vertical axis on the window plane. Successful power transmission was defined as ≥1.8V output from the receiving coil.

RESULTS: For positions where the receiving voltage was ≥1.8V (Fig. 3 dashed outline), the vertical transmitting coil height from the iTrapz receiver window (Separation) averaged less than 9.0±3.6mm and ranged from 5.5mm to 16.7mm. Average Alignment during the motion trials was 5.9±4.8 mm, ranging from 0.01mm to 14.2mm. However, within this coil position envelope (<16mm Separation and <14mm Alignment offset), where there was generally successful power transmission, there were also recordings where the output voltage was below 1.8V (Fig 3. dark blue). Additional measures of coil position are needed to fully describe the voltage distance-coupling relationship.

DISCUSSION: We present progress on the development of a trapezium replacement designed to measure *in vivo* loads across the thumb carpometacarpal joint. Here, we provide evidence that our design can be powered inductively, with a small (~20mm dia.) transmitting coil placed adjacent to dorsal surface of the base of the thumb. Additional design and testing iterations will be performed to optimize the envelope of threshold-level power transmission, and coil sizing. Once this is complete, and benchtop testing has been performed for structural and electrical integrity, the electrical components will be miniaturized, and fully functional prototypes will be produced for mechanical fatigue and hermetic seal testing.

SIGNIFICANCE/CLINICAL RELEVANCE: An instrumented trapezium capable of measuring kinetics at the base of the thumb will be immensely valuable to clinicians, researchers, and implant designers who need accurate joint loading data to understand the role of joint loading in thumb CMC joint pathophysiology, to refine musculoskeletal models, to standardize pre-clinical testing, and to develop more effective and cost-effective surgical treatments.

ACKNOWLEDGEMENTS: This research was funded in part by NIH/NIAMS R21AR077201.

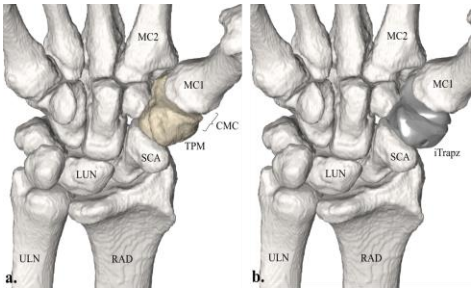

Fig. 1. Palmar view of the skeletal hand (a) segmented from a CT volume. The trapezium carpal bone (TPM) will be replaced with the load sensing iTrapz (b) in patients undergoing trapeziectomy for severe osteoarthritis.

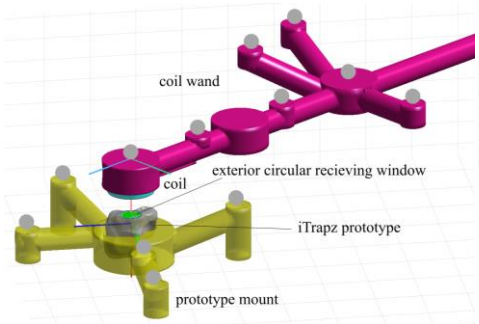

Fig. 2. 3D marker cluster appliances outfitted with optical motion capture markers (grey spheres). Optimally aligned (maximal transmission voltage = 4.9 V) reference position shown.

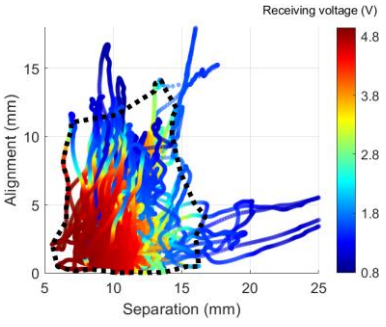

Fig. 3. Coil position during all motion trials quantified by Separation and Alignment, and colored by receiving voltage (color bar, V). Dashed black boundary depicts position envelope ≥1.8V.

Accuracy and Precision of Model-based Bone Tracking for a Dynamic Hop Landing Activity

John Holtgrewe[1], Braden C. Fleming[1], Jillian E. Beveridge[1]
[1]Brown University and Rhode Island Hospital, Providence, RI
Email of presenting author: john_holtgrewe@brown.edu

Disclosures: Braden C. Fleming (Miach Orthopaedics, American Journal of Sports Medicine); Other authors (N)

INTRODUCTION: Biplane videoradiography is commonly used to quantify 3D skeletal joint motion using either gold-standard marker-based tracking or the more clinically applicable model-based tracking. While model-based tracking depends only on the bone shape, it is more sensitive to biplane system geometry and bone-soft tissue image contrast. Our previous work demonstrated that the systematic errors of marker- vs. model-based bone tracking of individual cadaveric bone specimens are less than 0.25°/mm.[1] This information was critical to custom software development, but the uncertainty in 3D reconstruction of the kinematic position of relative bone movement as a function of in vivo biplane system geometry and realistic bone-soft tissue image contrast was not fully captured.[1] Given our interest in quantifying dynamic hop landing kinematics in patients following anterior cruciate ligament (ACL) surgery, we sought to quantify the accuracy, precision, and bias of model-based tibiofemoral kinematics relative to gold-standard marker-based tracking for a simulated hop landing task for a biplane system configuration used for in vivo motion capture.

METHODS: A male cadaveric knee specimen was used. Fourteen 0.80mm diameter tantalum beads were implanted: 6 in the distal femur and 8 in the proximal tibia. Computed tomography (CT) scans were taken, and femur and tibia models were generated using commercial software (Mimics; Materialise). To quantify precision of relative tibiofemoral bone motion, the specimen was frozen such that any non-zero joint motion was attributable to tracking errors. Three trials simulating a hop landing were recorded at 250 frames/second as the specimen was moved through the calibrated biplane system field of view. The average source to image distance for the biplane setup was ~185 cm, and the angle between the two x-ray image intensifier pairs was ~55°. X-rays were taken with a voltage of 76 kV and a current of 160 mA. Marker-based tracking was completed by digitizing and tracking the displacement of the beads in the x-ray videos using open-source software (XMALab; Brown University).[2] X-ray videos and model partial volumes were then processed to remove the spatial information associated with the beads using custom-written software.[3] Model-based tracking was then conducted using open source 2D-3D registration software (Autoscoper; Brown University).[4] Analyses were performed for each trial using the first 38 frames where both the femur and tibia were visible in the field of view. All tracking data were filtered using a 4th-order Butterworth filter. 3D knee motion was expressed as 6 degree of freedom (DOF) kinematics. For each DOF, the mean (± SD) absolute difference between marker- and model-based kinematics was used to describe tracking accuracy. Bland-Altman tests were used to quantify bias and precision.

RESULTS: The mean absolute differences in flexion/extension (FE), ab/adduction (AA), and internal/external (IE) rotation were 0.19±0.24°, 0.36±0.20°, and 0.64±0.55°, respectively. Translational differences in medial/lateral (ML), anterior/posterior (AP), and inferior/superior (IS) directions were 1.62±0.34mm, 0.20±0.26mm, and 0.14±0.09 mm, respectively. Bland-Altman analyses revealed biases of -0.07°, 0.24°, and 0.58° in FE, AA, and IE rotation respectively. Biases in the ML, AP, and IS translational DOFs were -1.60mm, 0.19mm, and -0.12mm, respectively. The Bland-Altman analysis also revealed limits of agreement (1.96xSD) of 0.59°, 0.66°, 1.2° for FE, AA, and IE rotation, respectively. Limits of agreement for ML, AP, and IS translation were 0.66mm, 0.51mm, and 0.23mm, respectively.

DISCUSSION: The accuracy, precision, and bias of 3D joint kinematics obtained from our hop landing biplane videography system configuration showed good agreement with previous measures based on idealized conditions, with the exception of some dependency on DOF of interest.[1] Of note, ML translation was the least accurate DOF (Fig 2) and is likely the result of ML translations occurring in the plane normal to the image intensifier (i.e., out-of-plane motion). This result was not unexpected given the geometry of our system was optimized to capture in-plane AP translation, in which model-based tracking was 8x more accurate compared to ML translation. We have previously reported that ACL reconstructed patients land with their tibia anteriorly translated by up to 7.5mm during a hop-landing compared to matched uninjured patients;[5] the magnitude of this difference is more than an order of magnitude greater than the level of imprecision quantified in the AP DOF here, giving us high confidence that our biplane videoradiography configuration and post-processing approach is sensitive to likely clinically meaningful long-term functional changes in this patient population of interest.

SIGNIFICANCE/CLINICAL RELEVANCE: The accuracy, precision, and bias of the biplane videoradiography configuration we have optimized to capture dynamic hop landing is sufficient to quantify what we believe are clinically relevant differences in 3D knee kinematics of ACL reconstruction patients, although caution should be used in interpreting dynamic medial/lateral tibial position.

REFERENCES: 1. Miranda, D. et al. J Biomech (133), 2011. 2. Knörlein, B. et al. J Exp Biol (219), 2016.
3. https://bitbucket.org/xromm/xromm_autoscopertools/src/master/ 4. Akhbari, B. et al. J Biomech (92), 2019. 5. Beveridge, JE. Et al. Trans ORS, 2020.

ACKNOWLEDGEMENTS: This project is supported by the NIH/NIAMS (K99/R00-AR069004, R01-AR047910, R01-AR074973), NIGMS (P30-GM122732, P20-GM139664) and the Lucy Lippitt Endowment.

IMAGES AND TABLES:

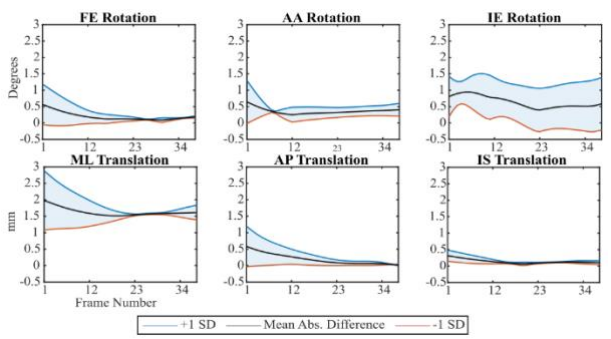

Figure 1 (left). Mean absolute difference between marker-based and model-based tracking by frame for each DOF.

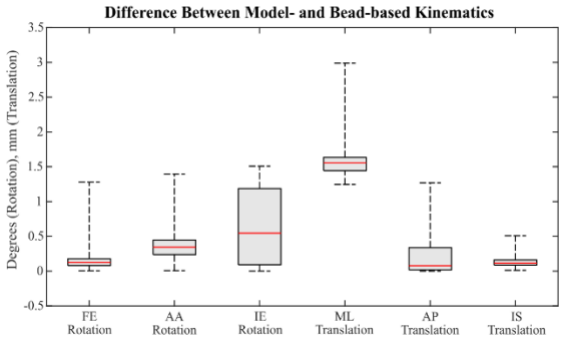

Figure 2 (right). Absolute difference between marker-based and model-based tracking by DOF.

Static and Dynamic Constraint in ACL-Reconstructed Patients at 10-15 Year Follow-Up

Jillian E. Beveridge[1], Madalyn Hague[1], Lauren R. Parola[1], Meggin Q. Costa[1], Janine Molino[2], and Braden C. Fleming[1]
[1]Department of Orthopedics, Rhode Island Hospital/Brown University, Providence, RI; [2]Lifespan Biostatics, Rhode Island Hospital, Providence, RI
jillian_beveridge@brown.edu

Disclosures: BCF: 4; MIACH Orthopaedics. 7B; American Journal of Sports Medicine. 8; American Journal of Sports Medicine. All other authors (N).

INTRODUCTION: The goal of anterior cruciate ligament reconstruction (ACLR) is to restore knee stability and reduce the risk of secondary damage to menisci and posttraumatic osteoarthritis (PTOA). Static laxity can be measured relatively easily and relates directly to the passive constraint conferred by ligaments (or grafts) and menisci. Conversely, dynamic kinematic outcomes are a combination of both passive constraint and the active constraint modulated by the neuromuscular system to provide joint stability. In both instances, the contralateral limb is almost always used as an internal control to represent baseline. In our work describing long-term joint function and the neuromuscular contributions to PTOA risk following ACLR,[1] we sought to explore the relationship between static and dynamic constraint in a subset of ACLR patients and control subjects who have been followed over a decade. The objective of the present work was to quantify bilateral static and dynamic tibiofemoral positions in ACLR patients and healthy controls. We hypothesized that anterior tibial position would be greater in the surgical compared to the contralateral knee and knees of control subjects, and that surgical limb differences in anterior tibial position would be greater in the dynamic state during a hop landing that challenges the ACL graft.

METHODS: Twenty-one subjects were recruited from the ongoing parent study [NCT00434837] and they provided written informed consent to participate in this IRB-approved ancillary study. Ten subjects (5 females/5 males; mean age=33.8±10.0 years; BMI = 26.9±4.2; 12.1±1.2 years follow-up) had undergone ACLR surgery 10-15 years prior to participation. Eleven control subjects (5 females/6 males, mean age=38.1±7.5 years; BMI = 24.3±3.2; 11.9±3.8 years post initial parent trial enrollment) were additionally recruited from the parent study. Femur and tibia bone models were segmented from computed tomography (CT) images that were obtained bilaterally, and local coordinate systems were generated automatically from the bone geometry.[2] The static 3D tibiofemoral position was extracted from the orientations of the bones in each subject's CT and described by 6-degree-of-freedom position to constitute our measure of "static constraint". Dynamic knee kinematics were recorded bilaterally at a frame rate of 250Hz using biplane videoradiography during a 1-leg hop landing that spanned ground contact to 0.2 seconds after. Side-to-side differences were used as a measure of "dynamic constraint". Peak anterior tibial position was the primary outcome measure for both static and dynamic conditions, and anterior tibial position as a function of dynamic flexion angle was the secondary outcome measure. Generalized estimating equations were used to test for differences between ACLR surgical and contralateral limbs, and between ACLR and controls. Pairwise comparisons between groups were tested within the models via orthogonal contrasts. The Holm test was used to adjust for multiple comparisons while maintaining a two-tailed alpha of 0.05. All analyses were conducted in SAS version 9.4 (SAS Institute Inc).

RESULTS: Whereas static flexion angles were consistent bilaterally in ACLR patients (p=0.82) and between ACLR patients and controls (p=0.20), static ACLR tibial position was significantly more anterior compared to uninjured controls (7.5±2.3mm; 95% CI [2.6-12.4mm], p=0.02) and the contralateral limb (3.1±1.1mm; 95% CI [0.77-5.4mm], p=0.04)(Fig. A, C). Knee flexion angle at peak anterior tibial position during the hop landing was also consistent bilaterally in ACLR patients (p=0.38) and between ACLR surgical knees and controls (p=0.90). Contrary to static position, the peak dynamic anterior position during the hop landing was not statistically different between surgical and contralateral limbs in ACLR patients (0.44±2.1mm; 95% CI [-4.0-4.9mm], p=0.83), but tended to be more anterior compared to controls (5.0±3.1mm, 95% CI [-1.44-11.5mm], p=0.12) (Fig. B). Dynamic anterior tibial position as a function of flexion angle (i.e., regression model slope) was similar between ACLR surgical limbs and controls (p=0.16), but the model intercept was 10.3mm greater in the ACLR surgical (95% CI [1.7-19.0mm]; p=0.01) and 7.5mm contralateral limbs (95% CI [1.8-13.2mm]; p=0.001) compared to controls.

DISCUSSION: Our hypothesis was supported whereby the tibia was significantly more anteriorly translated in ACLR patients in a static position which was maintained during dynamic function as demonstrated by the significant bias in anterior position despite a similar magnitude of anterior tibial translation with flexion as controls; however, we did not anticipate that the bias in ACLR anterior tibial position would be present bilaterally in the dynamic, but not static condition. The results suggest that ACLR patients have greater surgical limb static laxity, which aligns with conventional arthrometer measures in this population.[3] Conversely, dynamic stability was restored with no side-to-side differences. Nevertheless, the magnitude of both static and dynamic anterior tibial position bias compared to healthy controls was 5-7x greater than previously reported side-to-side differences within ACLR patients.[4] It is unknown whether the presence of dynamic bilateral symmetry represents "normal" function and could explain why these patients were at higher risk of injury, or whether the contralateral limb function changed due to central nervous system adaptations to restore stability and symmetry.[5] Future longitudinal studies would be needed to answer this question.

SIGNIFICANCE/CLINICAL RELEVANCE: Static laxity is present long after ACLR, whereas dynamic side-to-side stability is restored but with a persistent bias towards greater anterior tibial position that is present bilaterally. The stark contrast between static and dynamic constraint was detectible only in the context of healthy control data, emphasizing the caution needed in treating the contralateral limb as "normal" in ACLR patients.

REFERENCES: 1. Zandiyeh, P. et al. Bioeng J. (2023); 2. Miranda, D. et al. J Biomec (2011); 3. Akelman, M. et al. AJSM (2016). 4. Deneweth J. et al. AJSM (2010). 5. Needle, A. et al. Sports Med (2017).

ACKNOWLEDGEMENTS: NIH NIAMS (K99/R00-AR069004, R01-AR047910, R01-AR074973); NIGMS (P30-GM122732, P20-GM139664); and the Lucy Lippitt Endowment.

IMAGES AND TABLES:

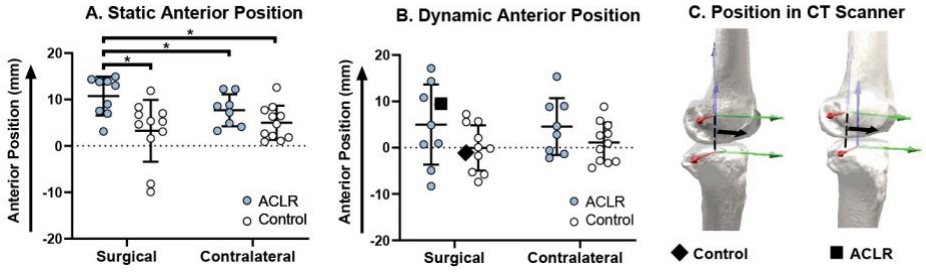

Figure. A. *Static anterior tibial position. "*" denotes statistically significant.* ***B.*** *Peak anterior tibial position during hop landing. The square and diamond correspond to the individual subjects shown in (C).* ***C.*** *Visualization of anterior tibial position for examplar subjects; local coordinate system axis orientations are displayed by red (medial-lateral), green (anterior-posterior), and blue (inferior-superior) arrows.*